# AUTHOR QUERY FORM

| | | |
|---|---|---|
| ELSEVIER | **Journal:** EA<br><br>**Article Number:** 16768 | **Please e-mail or fax your responses and any corrections to:**<br><br>**E-mail:** corrections.esil@elsevier.thomsondigital.com<br><br>**Fax:** +353 6170 9272 |

Dear Author,

Please check your proof carefully and mark all corrections at the appropriate place in the proof (e.g., by using on-screen annotation in the PDF file) or compile them in a separate list. To ensure fast publication of your paper please return your corrections within 48 hours.

For correction or revision of any artwork, please consult http://www.elsevier.com/artworkinstructions.

Any queries or remarks that have arisen during the processing of your manuscript are listed below and highlighted by flags in the proof. Click on the 'Q' link to go to the location in the proof.

| Location in article | Query / Remark: click on the Q link to go<br>Please insert your reply or correction at the corresponding line in the proof |
|---|---|
| | Please complete and update the reference given here (preferably with a DOI if the publication data are not known): [41].<br>For references to articles that are to be included in the same (special) issue, please add the words 'this issue' wherever this occurs in the list and, if appropriate, in the text. |
| Q1 | Please update Ref. [41]. |
| Q2 | Figs. 3–5 will appear in black and white in print and in color on the web. Based on this, the respective figure captions have been updated. Please check, and correct if necessary. |

Thank you for your assistance.

Electrochimica Acta xx (2011) xxx–xxx

Contents lists available at ScienceDirect

Electrochimica Acta

journal homepage: www.elsevier.com/locate/electacta

Research highlights

*Electrochimica Acta xx (2011) xxx–xxx*

**Optimal self-organized growth of small anodic $TiO_2$ nanotubes with "micro-annealing" effect under complex conditions via reaction–diffusion approach**

H. Liu, L. Tao, W.Z. Shen*

► Nonmonotonous size evolution of anodic $TiO_2$ tubes under low temperatures. ► New approach to a general mechanism of the size evolution. ► Formation of nanocrystal $TiO_2$ in the anodic tubes by temperature controlling. ► High speed growth of small sized $TiO_2$ tubes with better structural ordering.

Electrochimica Acta xxx (2011) xxx–xxx

Contents lists available at ScienceDirect

Electrochimica Acta

journal homepage: www.elsevier.com/locate/electacta

# Optimal self-organized growth of small anodic $TiO_2$ nanotubes with "micro-annealing" effect under complex conditions via reaction–diffusion approach

H. Liu, L. Tao, W.Z. Shen*

*Laboratory of Condensed Matter Spectroscopy and Opto-Electronic Physics, Key Laboratory of Artificial Structures and Quantum Control (Ministry of Education), Department of Physics, Institute of Solar Energy, Shanghai Jiao Tong University, 800 Dong Chuan Road, Shanghai 200240, People's Republic of China*

ARTICLE INFO

*Article history:*
Received 28 October 2010
Received in revised form 3 February 2011
Accepted 4 February 2011
Available online xxx

*Keywords:*
Anodic $TiO_2$ nanotube
Complex condition
Optimal growth
Ultrasmall tube
Reaction–diffusion method
Partial crystallization
Micro-annealing

ABSTRACT

This work investigates the change of the morphology and the structural characteristics of the anodic $TiO_2$ nanotubes under complex conditions (the temperature and the applied potential difference). Optimal growth for small tubes with specific sizes has been realized during this investigation, for example, high quality uniform ultrasmall (outer diameter $D \sim 10$ nm, wall thickness $d \sim 3$ nm) tubes can be grown without sacrifice of the growth rate (0.3–0.4 μm $h^{-1}$). A mechanistic description to the nonmonotonous morphology change under low temperatures has been approached with reaction–diffusion method considering the local reaction, diffusion and field drift processes of the main reaction species. We have also investigated the details of the partial crystallization in the as-prepared $TiO_2$ tubes and discovered its strong relationship with the temperature. Due to its similarity to the thermo annealing up to several hundred centigrade but much smaller length scale, this phenomenon is named as "micro-annealing" effect.



## 1. Introduction

$TiO_2$ nanotubes fabricated by anodic oxidation have received tremendous attention for their excellent optical and electronic characteristics and photocatalytic ability, making them a suitable material for wide spread range of applications such as dye-sensitized solar cells (DSSCs) [1,2], photocatalysis [3,4], electrochromic display devices [5], and biomedical uses [6]. It has been found that the morphological and structural characteristics of the $TiO_2$ tube arrays can significantly modify their optical or electronic properties and thus influence their performance in devices. For example, the band gap of $TiO_2$ may shift several $10^{-1}$ eVs with the existence of small crystal grains inside, while when grains are small enough, certain quantum size effect may also be induced as a result [7–10]. Furthermore, in real applications, the conversion efficiency can be significantly increased with smaller $TiO_2$ nanotubes in DSSCs [11,12].

Such findings on the characteristic modification of the nanostructured $TiO_2$ materials indicate the importance to study the controlling method and detailed mechanism during the fabricating process, and for such purpose many results have been obtained [13–18]. As a preliminary helpful basis, the application of viscous organic electrolyte and slow initial potential ramping has greatly improved the quality of the $TiO_2$ nanotube arrays with ultrahigh aspect ratio [19–22]. The size (in- and outer diameter, wall thickness, pore distances, etc.) controlling has been studied from different ways, such as the electrolyte type [23,24], the water effect [22,25–27] and the applied potential difference [28–30]. Some new morphological and structural behaviors have also been found under different conditions, such as the "bamboo type" structure between the tubes and the "nanolace" structure [31,32]. More recently, it has been reported that nanocrystal grains were formed during the anodization under certain condition [33,34,46] without the conventional thermo annealing of $TiO_2$ up to several hundred centigrade for anatase phased crystal structure [33,35].

However, in the realistic self-organized systems, the structure formation is always cooperation of different factors under quite complicate boundary conditions on the substrate. Therefore adjustment with combined different factors will be needed for the optimized growth of tubes with specific size (in- and outer diameter, wall thickness) and adequate quality. Furthermore, more details in the mechanistic description on the $TiO_2$ tube growth remain still unclear, such as the morphological behavior of the tube formation under realistic conditions (temperature, applied potential, boundary condition of the substrate, etc.). Consequently, it is

* Corresponding author. Fax: +86 21 54747552.
*E-mail address:* wzshen@sjtu.edu.cn (W.Z. Shen).

0013-4686/$ – see front matter © 2011 Published by Elsevier Ltd.
doi:10.1016/j.electacta.2011.02.029

necessary to probe the system in some different way. Fortunately, the reaction–diffusion method has been proved a good tool to investigate the self-organized systems with complicate boundary conditions and employed in electrochemistry and heterogeneous catalysis [36–39]. Dynamical studies have also shown that beside the anodic potential and the electrolyte, the temperature is also an important factor that significantly influences the diffusivity and reaction rate in the system [36,40–42], thus might also consequently influence the tube formation.

In this work, the anodic growth of $TiO_2$ nanotubes in ethylene glycol (E.G., containing 1.0 vol.% $H_2O$) has shown nonmonotonous morphological changes when varying the temperature and the applied potential difference in a wide range. Small tubes can also be formed at high applied potential difference under low temperature, with much faster growth rate than the normal low voltage growth at room temperature where the tube size is approximately linearly proportional to the applied potential difference [20,43]. Thus the optimized conditions to grow small $TiO_2$ tubes with specific sizes are determined through tuning of the temperature and the applied potential. A mechanistic explanation of the general behavior is approached by applying the reaction–diffusion method with consideration of the reaction, diffusion, and field drift processes of three key species: $F^-$, $O^{2-}$ and $TiO_2$.

Structural characterization has also been carried out to investigate the as-prepared $TiO_2$ tubes under such conditions. The partial crystallization discovered in the as-prepared $TiO_2$ tubes shows strong relationship with the total heat effect from the reaction and the current flow and the temperature gradient from the anode cell to the electrolyte. Due to its similarity to the annealing to several hundred centigrade but much smaller length scale, this phenomenon is named "micro-annealing", which might be useful in general nanostructure fabrication. Considering those phenomena, it is expectable to fabricate uniform small $TiO_2$ tubes with high growth rate and as-grown structural ordering in some degree by properly controlling some simple conditions.

## 2. Experimental

The titanium foils we used in this study are 0.25 mm thick and 99.7% purity (Sigma–Aldrich and Alfa-Aesar). Before the anodization, they were cleaned with ultrasonic bath in acetone, isopropanol, methanol, and ethanol, respectively, followed by subsequent rinsing in de-ionized water and drying with air. The anodic oxidation was performed in a two-electrode configuration using a direct current power supply (Agilent 5720), in which a copper plate was used as the cathode and a Keithley 2400 sourcemeter to measure the resulted current. Anodizing was undertaken in quiescent solution of 0.09 M $NH_4F$ in de-ionized water and E.G. To obtain high aspect ratio and tube quality, the water concentration in the solution was 1.0 vol.% and the applied potential difference was ranged from 0 to 330 V. All electrolytes were prepared from reagent grade chemicals. The anodization includes an initial potential ramping and afterwards a constant applied potential for 1 h, with constant stirring rate at 400 rpm. Finally, the accurate temperature control was conducted by a thermostatic bath.

The as-prepared $TiO_2$ nanotube arrays were rinsed with de-ionized water and dried in air spontaneously after the experiments. Their morphology and structure were characterized by a field-emission scanning electron microscope (FE-SEM; Philips XL30FEG) with an accelerating voltage of 5 kV. The detailed microstructures of the tubes were studied by a transmission electron microscopy (TEM, JEOL JEM2100), with 200 kV accelerating voltage. The crystalline information is also studied by Raman spectroscopy in a Jobin Yvon LabRAM HR 800UV micro-Raman system. The Raman spectra were recorded in backscattering configuration using an exciting wavelength of 514.5 nm from an $Ar^+$ laser.

## 3. Results and discussion

### 3.1. Morphological study of the $TiO_2$ nanotube formation under complex conditions

In order to approach more realistic $TiO_2$ electrochemical growth, we have carried out a new systematic morphological investigation under complex conditions (the temperature and the total applied potential difference $\Delta V$) below room temperature (defined as 20 °C). The first significant phenomenon is the shift of the boundary conditions for the tube formation. With decreasing temperature, the upper limit of $\Delta V$ at which tubes can be formed significantly shifted to higher voltage side, which is interesting compared to the $TiO_2$ experiments normally carried out near or above room temperature [14–18,27,29,31,33]. The upper limit of the applied potential difference is indicated as the edge of the valleys in upper right side in Fig. 1(a)–(c), which have shown the $\Delta V$–$T$ diagrams of tube outer diameter ($D$), wall thickness ($d$), and tube length ($L$) (grown in 1 h), respectively. As an example, at 15 °C, the upper limit of $\Delta V$ was 210 V, while at 5 °C, it became 330 V.

Secondly, the morphology of the tubes has some sophisticated change under the complex conditions in a wide range. At constant temperature, the tube outer diameter $D$ and wall thickness $d$ did not change monotonously with the applied potential difference, as shown in the diagrams in Fig. 1(a). When the temperature became lower, this behavior became more significant. For example, at 5 °C, the tube outer diameter first increased with $\Delta V$, reached maximum (~320 nm) at 210 V, and then again decreased with the increasing $\Delta V$, as also shown by SEM images in Fig. 1(d)–(i). This is different compared to the monotonous behavior of diameter $D$ versus the applied potential difference at room temperature, which has been described by $D = 2f_{growth}\Delta V$, with the growth factor $f_{growth} = t_{film}/\Delta U'$ ($t_{film}$ is the compact oxide thickness in Ti at a certain voltage drop $\Delta U'$) [11,20,43]. Beside the outer diameter, the tube wall thickness and tube length also changed nonmonotonously with the applied potential difference at low temperatures, also different from the result at room temperature for the system with the same electrolyte concentration.

Moreover, the morphological change of the system becomes more complicate at fixed applied potential difference $\Delta V$, but the general tendency can still be extracted out. The tube diameter and wall thickness were generally less at lower temperature, as shown in Fig. 1(a) and (b). At low enough $\Delta V$ (~10 V) and temperature (~0 °C), the tube size reached minimum ($D \sim 10$ nm and $d \sim 3$ nm). In the meanwhile, the nanotube still grew quite fast under temperatures around 0 °C, as shown in Fig. 1(c). And under some conditions the growth rate can even be higher than that at room temperature, for example, under 5 °C at 210 V, the tube length can reach ~113 nm, longer than the length obtained under room temperature at the same applied potential. Considering the negative effect of low temperature on reaction rate and diffusivities of species, it will be interesting to study the mechanism of the anodization process under low temperature.

The above facts have suggested a way to grow ultrasmall tubes ($D \sim 10$ nm, $d \sim 3$ nm) with fast growth rate (0.3–0.4 $\mu m\,h^{-1}$) by controlling the temperature and the applied potential difference $\Delta V$ together properly. With controlled complex conditions, small tubes (50–90 nm) can be also grown with fast growth rate at high $\Delta V$ due to the nonmonotonous size evolution versus $\Delta V$ under fixed low temperature. For example, tubes with $D \sim 80$ nm and $d \sim 30$ nm are normally obtained at 30 V under room temperature and at 40 V under 5 °C with the growth rate less than 2.5 $\mu m\,h^{-1}$,



Please cite this article in press as: H. Liu, et al., Optimal self-organized growth of small anodic $TiO_2$ nanotubes with "micro-annealing" effect under complex conditions via reaction–diffusion approach, Electrochim. Acta (2011), doi:10.1016/j.electacta.2011.02.029

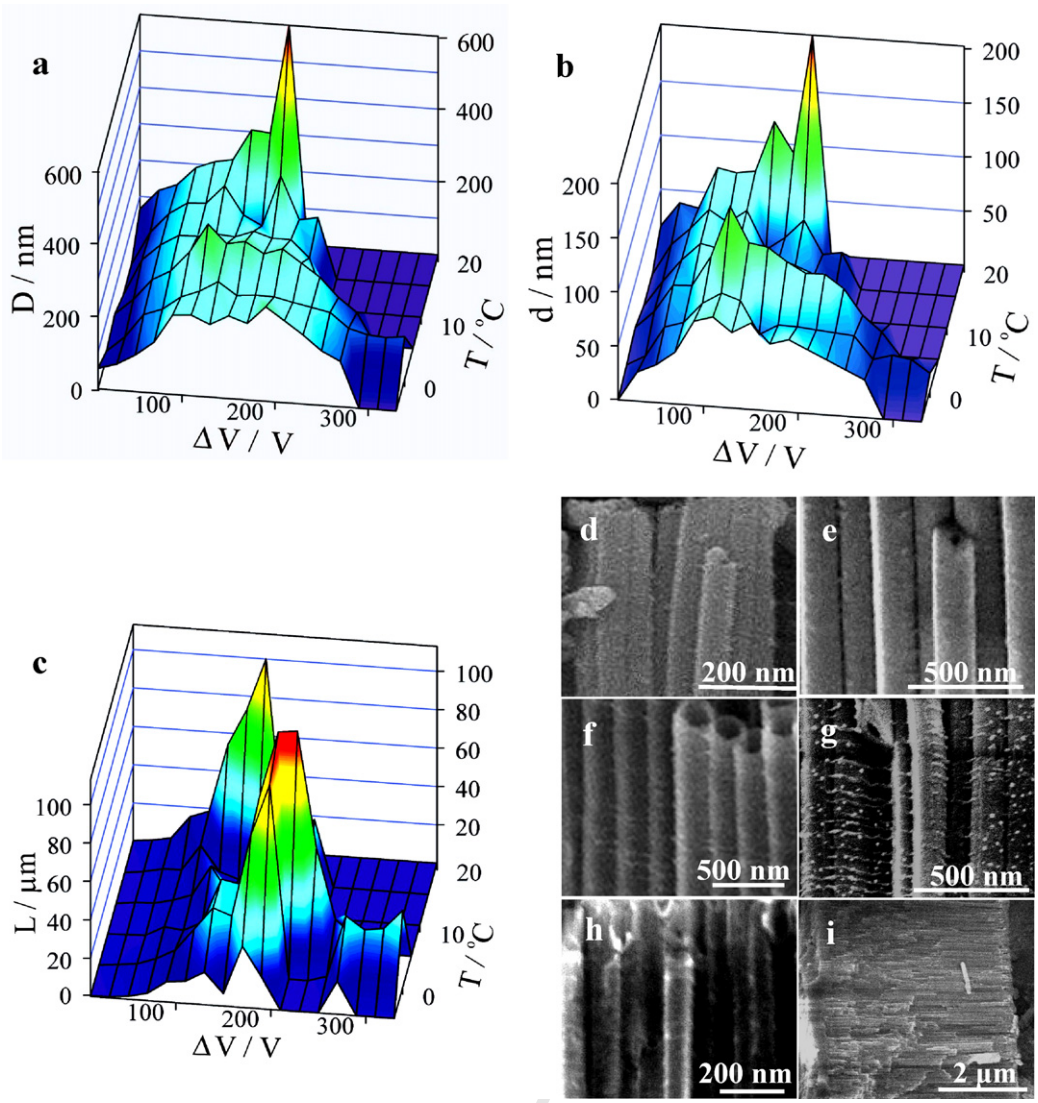


**Fig. 1.** Behavior of the $TiO_2$ tube formation at low temperature region versus the applied potential difference $\Delta V$ in ethylene glycol, 0.09 M $NH_4F$, 1.0 vol.% $H_2O$, and 1 h anodization time. (a)–(c) Phase diagrams versus temperature and the applied potential difference: (a) outer diameter *D*, (b) wall thickness *d*, and (c) tube length *L*. (d)–(i) Nonmonotonous size evolution with increasing applied potential difference, shown by SEM images of $TiO_2$ tubes formed at 5 °C: (d) 20 V, (e) 150 V, (f) 210 V, (g) 240 V, (h) 280 V, and (i) 280 V, showing the total length.

while the same tubes can also be fabricated with thinner wall (~15 nm) at growth rate ~6 μm $h^{-1}$ by 280 V at 5 °C, as exhibited by the SEM images in Fig. 1(h) and (i). It can also be noticed that those behaviors have shown quite intricate nature of the $TiO_2$ anodic system, whose mechanism might therefore need consideration of more detailed factors, such as, the temperature influence on activation energy of reaction and diffusion, the diffusion of ion species in the tubes, and the field drift of the species by the anodic potential.

### 3.2. Micro-annealing effect of the $TiO_2$ tubes with temperature controlling

According to the experiments mentioned in Section 3.1, the $TiO_2$ anodic oxidation system has shown interesting morphological behavior in a wide condition range. It is therefore necessary to investigate if there is possible structural change. As normally known, the as-prepared $TiO_2$ nanotubes are normally formed as amorphous $TiO_2$ at room temperature [19,33,35]. However, as being recently reported, some nanocrystal grains can be formed in the as-prepared anodic $TiO_2$ tubes [33,34], but the detailed behavior and decisive factors are still not very clear.

In our experiments, it was confirmed that this phenomenon is reproducible, and is very likely to be related to the temperature. It was found that when temperature was getting down, more small $TiO_2$ grains with ordered microstructure were formed inside the tube wall. As shown in Fig. 2(a), tubes under 15 °C were still mostly amorphous, while in some places marked by red arrows, atoms tended to become organized. However, at lower temperatures, for example, 5 °C as shown in Fig. 2(b), many small grains with the size normally of 2–10 nm almost occupied the tube wall with the atomic distance 0.35–0.38 nm, which is close to the lattice constant of anatase (*a*: 0.378 nm, *c*: 0.951 nm) [44]. When temperature was further lowered, even more grains would be formed that can almost occupy the tube walls.

Since the detection area of TEM is somehow limited to a small scale, it is necessary to use technique like Raman spectroscopy to detect information of larger scales. Fig. 2(c) represents the Raman spectra for the $TiO_2$ tubes under different temperatures. They clearly shows that at higher temperature (15 °C), the $TiO_2$ is mostly amorphous like, while at lower temperature, the characteristic Raman peaks become significantly stronger, which are mostly related to nanocrystal $TiO_2$ grains [45]. The



Please cite this article in press as: H. Liu, et al., Optimal self-organized growth of small anodic $TiO_2$ nanotubes with "micro-annealing" effect under complex conditions via reaction–diffusion approach, Electrochim. Acta (2011), doi:10.1016/j.electacta.2011.02.029

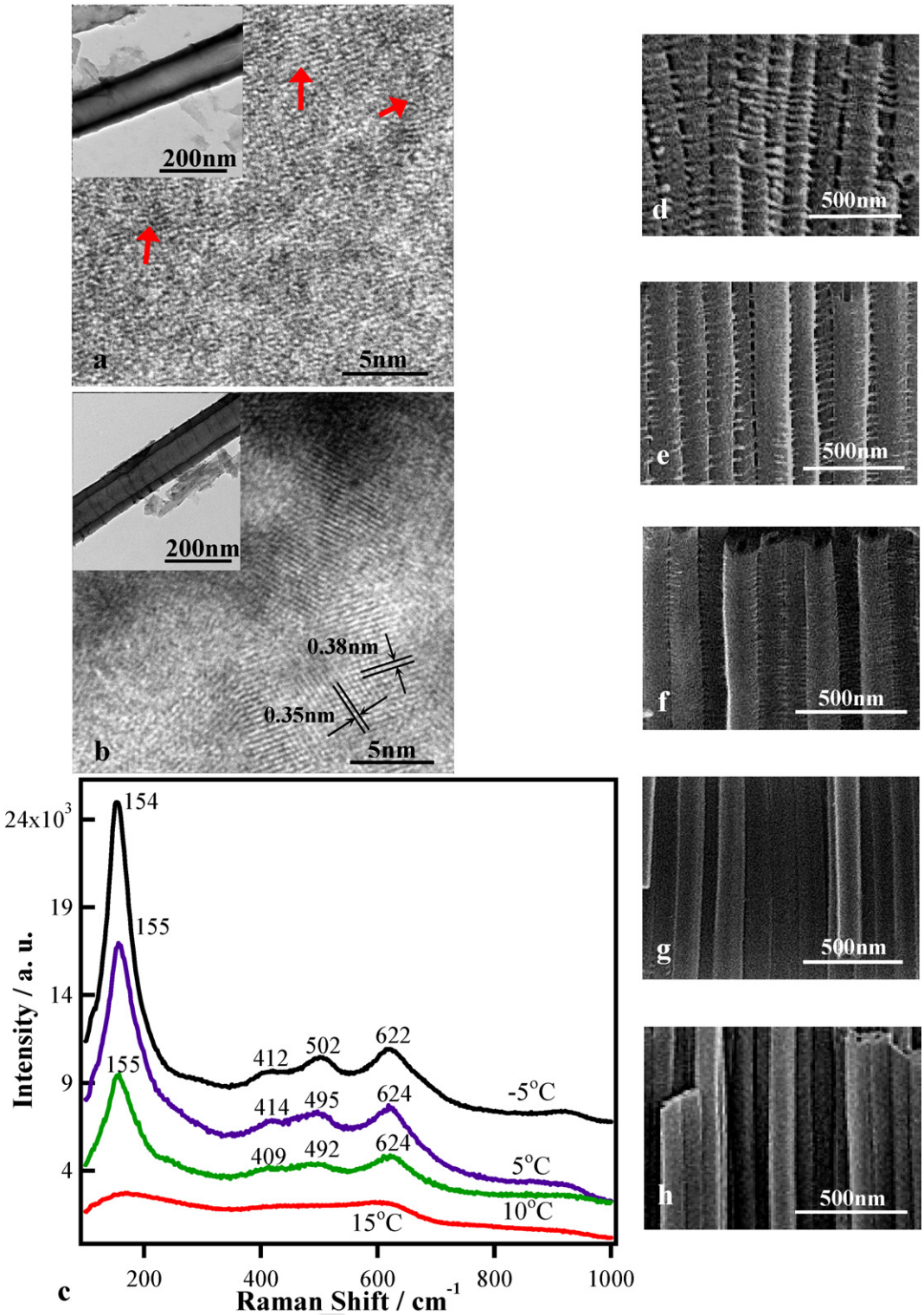


**Fig. 2.** "Micro-annealing" and ordering effect under low temperatures. High resolution TEM images of $TiO_2$ tubes under (a) 15 °C and (b) 5 °C at 210 V, showing formation of small grains with decreasing temperature, the inset is the whole view. (c) Raman spectra of $TiO_2$ tubes obtained at different temperatures of −5 °C, 5 °C, 10 °C, and 15 °C at 210 V. (d)–(h) SEM images showing ordering and smoothness change with different temperatures of (d) 15 °C, (e) 10 °C, (f) 5 °C, (g) 0 °C, and (h) −5 °C at 70 V.

structures at 155, 492, and 624 $cm^{-1}$ under 10 °C, 155, 495, and 624 $cm^{-1}$ under 5 °C and 154, 502, and 622 $cm^{-1}$ under −5 °C are due to the anatase phased grains, and those of 409 $cm^{-1}$ under 10 °C, 414 $cm^{-1}$ under 5 °C and 412 $cm^{-1}$ under −5 °C from the rutile phased ones The significant enhancement of the Raman intensity from 10 to −5 °C clearly indicates the increase of the nanocrystal grains versus the amorphous contents inside those tubes, accompanied by the slight shift of the peak positions. In addition, beside the changes in the microstructure in the tube walls, the quality of tubes in the array is also improved with decreasing temperature. The tubes are normally better organized under lower temperatures, as shown in Fig. 2(d)–(h),

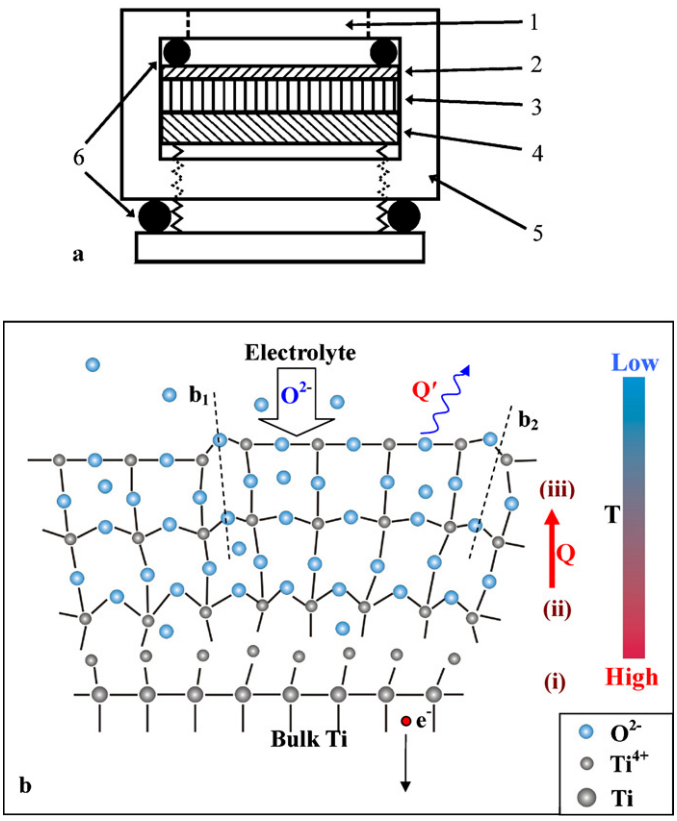


**Fig. 3.** Schematic illustration of "micro-annealing" effect in as-prepared $TiO_2$ tubes under low temperature: (a) overview of the anode structure: 1 – opening window, 2 – Ti plate, 3 – copper electrode, 4 – copper plate, 5 – outer shell, 6 – rubber O-ring. (b) The "micro-annealing" process. $V$ is the potential applied on the anode, $b_1$ and $b_2$ indicate the boundaries between the formed grains, $Q$ is the heat produced by the reaction and current flow that activate the crystallization, $Q'$ is the heat released when local crystallization is finished, the color bar to the right side shows the temperature ($T$) gradient, and (i)–(iii) represent the key steps. (For interpretation of the references to color in this figure legend, the reader is referred to the web version of this article.)

which will be helpful in the realistic application in optoelectronic devices.

The experimental results indicate that the temperature has played an important role in the formation of ordered structures in the $TiO_2$ tube walls. Hence we will interpret the process with consideration of the heat effect and structure of the anode. First of all, the anodic growth of $TiO_2$ nanotube is a non-equilibrium system, so the heat will be continuously generated until the growth is stopped. Secondly, according to the structure of the anode shown in Fig. 3(a), one side of the Ti plate is in contact with the Cu electrode surrounded by plastic chamber wall with relatively lower heat conductance than Ti and Cu metal and another side of the Ti plate is open to the electrolyte kept at constant low temperature. Therefore the temperature distribution over the oxide layer and Ti substrate will not be homogeneous even across such a small length scale (~0.25 mm). From the electrolyte side to the electrode side, the temperature gradient will be positive.

The joule heat during the whole process may come from two origins: the reaction and the current flow $I$, so the total heat can be described by $Q = \sum \Delta H_i + \Delta V_a I$, where $\sum \Delta H_i$ is the sum of the enthalpies from the chemical reactions and $\Delta V_a$ is the potential drop over the near-anode region [46]. The direct calculation of the total joule heat is difficult because of two reasons: first, the detailed elementary steps of all the reactions are still unclear; second, the ohmic resistance of the path that the current flow through is changing during the tube growth. However, the overall heat effect can be detected during the experiments. During the reaction, there was a significant temperature rise (~60 °C at 160 V) in the anode, while the side of Ti plate exposed to the electrolyte was kept at low temperature by constant stirring. This is just the heat effect that has been transferred out to the surface of the plastic anode chamber. It means at the sample layer with very thin thickness (≪0.25 mm), there can be more energy distributed to the as-formed amorphous $TiO_2$ per mole, which is enough for the activation energy for crystallization.

As shown in Fig. 3b, the process may consist of several main steps (i)–(iii). Firstly, the titanium atoms are initially oxidized to interstitial $Ti^{4+}$ cations by the anodic electric field [29], which are excited from their original position in the Ti lattice, as shown in step (i) of Fig. 3(b). In the step (ii), the $Ti^{4+}$ cations are combined with the $O^{2-}$ anions that diffuse through the oxide layer, thus amorphous Ti oxide is formed and certain heat is generated by the reaction. In the mean time, the current flow through the sample also produces heat. During a short time period, the total heat $Q$ will be distributed to the local as-formed amorphous Ti oxide. The amorphous oxide is excited to overcome the activation energy for annealing, then it releases certain heat ($Q'$) and become crystallized due to the relatively lower temperature at the electrolyte/$TiO_2$ interface, as indicated in Fig. 3(b) by step (iii). At lower electrolyte temperature, the crystallization will be enhanced. And since the $TiO_2$ grains were soon surrounded by the low temperature electrolyte and the heat conductance of $TiO_2$ is low, the size of the grains is therefore limited.

Overall, the temperature plays an important role in two factors: (1) the local temperature rise by heat released from reaction and current, which gives energy to the as-formed amorphous Ti Oxide to overcome the activation energy for the crystallization; (2) the gradually decreasing temperature from the inside of the anode to the electrolyte, which induces the crystallization and limit the size of the crystal grains. Due to the existence of the $F^-$ ions that dissolve part of the formed $TiO_2$ and form tubular structure, the formation and partial crystallization of $TiO_2$ will continue until all Ti is consumed or the growth is manually stopped. It is the reason to induce a macroscopic effect that small grains can fill the whole tube array despite that the crystallization itself is localized. Consequently, we name this effect "micro-annealing" effect due to the important role of temperature and the small length scale compared to the thermo annealing up to several hundred centigrade. It indicates a way to improve the ordering in the microstructure of nanostructure material by electrochemical method in the early steps during the fabrication.

### 3.3. Mechanistic description of the anodic growth of $TiO_2$ nanotubes with reaction–diffusion method

In the experimental studies of this work, the $TiO_2$ anodic system has shown quite sophisticated morphological behaviors, especially the nonmonotonous change in size (in- and outer diameter, wall thickness) and growth rate with varied applied potential difference and temperature (below room temperature). For the mechanism explanation, more detailed steps are possibly necessary to be considered. As well known, during the growth of $TiO_2$ nanotubes by anodization, there are two main general reactions:

$$Ti + 2H_2O \rightarrow TiO_2 + 4H^+ + 4e^- \quad (1)$$

$$TiO_2 + 4H^+ + 6F^- \rightarrow TiF_6^{2-} + 2H_2O \quad (2)$$

For a more detailed description of the process, we considered the reaction–diffusion model which has been applied for systems of heterogeneous catalysis and electrolysis [36–39], in which the concentration of the species at a certain position in real space is determined by local chemical reaction, diffusion of the species and



Please cite this article in press as: H. Liu, et al., Optimal self-organized growth of small anodic $TiO_2$ nanotubes with "micro-annealing" effect under complex conditions via reaction–diffusion approach, Electrochim. Acta (2011), doi:10.1016/j.electacta.2011.02.029

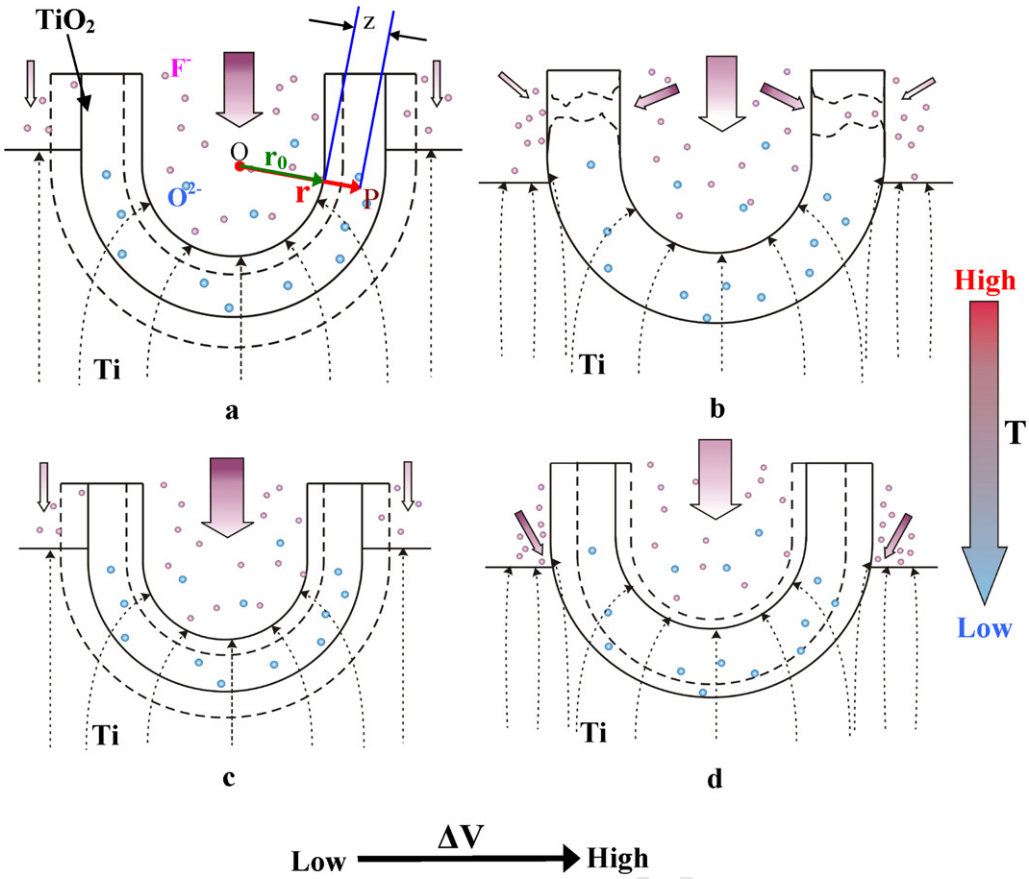


**Fig. 4.** Schematic diagram of $TiO_2$ tube formation at different temperatures and applied potential differences ($\Delta V$): (a) room temperature and low $\Delta V$, where O is the center of coordination, **r** is the coordinate vector, $r_0$ the inner radius, P is the point to investigate, and $z$ is the depth of P through the oxide layer. Two dashed curves indicate the change of the $TiO_2$ inner and outer surface with a rise in $\Delta V$; (b) room temperature and high $\Delta V$. The irregular dashed curves in the wall indicate the side etching on the tube wall that forms porous structures; (c) low temperature and low $\Delta V$; and (d) low temperature and high $\Delta V$. Inner and outer dashed curves indicate the change of the $TiO_2$ inner and outer surface with a rise in $\Delta V$. Big and small purple arrows denote the flow of $F^-$ ions, with their color gradient denotes the concentration intensity. Dashed curved arrows indicate the distributed electric field in the oxide layer and substrate. (For interpretation of the references to color in this figure legend, the reader is referred to the web version of this article.)

the field-assisted drift. Thus the following reaction–diffusion equations are built:

$$\frac{\partial[F^-]}{\partial t} = -k_1 R_1([TiO_2],[F^-]) + D_{F^-}\nabla^2[F^-] + \sigma_{F^-}[F^-]\nabla E \quad (3)$$

$$\frac{\partial[O^{2-}]}{\partial t} = -k_2 R_2([Ti^{4+}],[O^{2-}]) + D_{O^{2-}}\nabla^2[O^{2-}] + \sigma_{O^{2-}}[O^{2-}]\nabla E \quad (4)$$

$$\frac{\partial[TiO_2]}{\partial t} = \frac{1}{2}k_2 R_2([Ti^{4+}],[O^{2-}]) - \frac{1}{6}k_1 R_1([TiO_2],[F^-]) \quad (5)$$

Here the water effect has not been considered since the system in the present work only contains small $H_2O$ content (1.0 vol.% $H_2O$) [22,25–27]. The process is schematically illustrated in Fig. 4(a)–(d). The bottom of the tube is the mostly important part in the discussion of the tube morphological behavior. In this model, we apply a special 1D coordination system due to the symmetric shape of the tube bottom. The origin of coordination is the center of curvature of the inner surface of the tube bottom (point O in Fig. 4 (a)). Since the tube bottom is approximately round shaped, the center of curvature of the bottom is unique at a certain time. The coordinate vector **r** starts from the center to the point under investigation (point P), as shown by the red arrow in Fig. 4(a). Then the whole bottom of the tube can be described by a series of 1D system with different pointing angles with the reference frame moving along with the growth of the tube.

Eqs. (3)–(5) denote the concentration change of the species $F^-$, $O^{2-}$, and $TiO_2$ at a certain position in the oxide layer, respectively, and for simplification, $TiO_2$ is treated as single particle. The first terms in Eqs. (3) and (4) represent the reaction rates of the $TiO_2$ dissolution and Ti oxidation process with rate coefficient $k_1$ and $k_2$, respectively. $R_1([TiO_2],[F^-])$ and $R_2([Ti^{4+}],[O^{2-}])$ are two functions of reactant concentrations whose actual forms depend on the elementary steps of the Ti anodic oxidation and $TiO_2$ dissolution processes, which are still not clear according to current researches. The second terms in Eqs. (3) and (4) stand for the diffusion terms of the ions through the oxide with $D_{F^-}$ and $D_{O^{2-}}$ the diffusion coefficients. The third terms in Eqs. (3) and (4) represent the ion drift by electric forces, with $\sigma_{F^-}$ and $\sigma_{O^{2-}}$ the ionic mobility in the electrolyte or in the oxide. In the 1D coordination system applied here, vectors have only two directions: toward or away from the center of coordination O. Therefore the gradient of the potential $\nabla E$ can be scalarized with their sign representing the direction of the field drift effect on the ions. Eq. (5) indicates the change of the local $TiO_2$ concentration determined by the oxidation (first term) and dissolution (second term) processes, with $TiO_2$ treated as one whole particle. Eqs. (3)–(5) can normally only be numerically simulated due to the normally nonlinear reaction terms inside. Due to the lack of actual forms of the reaction terms by current knowledge, it is still difficult to make simulations with mathematical tools. However, we can consider an already stable tube growth and study the change of parameters induced by the key experimental factors, thus a mech-



Please cite this article in press as: H. Liu, et al., Optimal self-organized growth of small anodic $TiO_2$ nanotubes with "micro-annealing" effect under complex conditions via reaction–diffusion approach, Electrochim. Acta (2011), doi:10.1016/j.electacta.2011.02.029

anistic description of some general phenomena is possible to be sketched out.

For the rate coefficient $k_1$, there is normally a relationship $k_1 \sim \exp(-E_a/k_BT)$, where $E_a$ is the activation energy of the dissolution process. And for the oxidation process, there is a relationship $k_2 \sim \exp(-E_a'/k_BT)\exp(\beta zF\Delta V_s/k_BT)$ according to previous works from Bessler [36], where $E_a'$ is the activation energy for the oxidation, $\beta$ is the symmetry factor, $z$ is the number of transferred electrons per oxidized Ti atom, $F$ is the Faraday's constant and $\Delta V_s$ the overpotential on the sample. It indicates that compared to the dissolution process, the oxidation process is more sensitive to the change of the applied potential difference. Consider the diffusion term, as well known, the diffusion coefficient normally has the form $D_0\exp(-E_{ad}/k_BT)$ [42], with $E_{ad}$ the activation energy for diffusion. Furthermore, the viscosity of ethylene glycol changes quite sensitively with decreasing temperature. For example, the viscosity of pure ethylene glycol at 20 and 0 °C are 0.021 and 0.063 kg m$^{-1}$ s$^{-1}$, respectively, as calculated from scientific resource [47]. As a result, the ionic mobility $\sigma_{F^-}$ and $\sigma_{O^{2-}}$ are strongly influenced by the temperature change [48].

Assume that a stable growth has already been established, then tubes grow with a certain inner and outer diameter, thus also a stable thickness $d$. In the moving frame coordination, the relative position of the inner and outer surface of $TiO_2$ with the coordination center is fixed, thus the intersection point of coordinate vector $\mathbf{r}$ with those surfaces is fixed. Define $z$ as the distance of the point to be investigated (point P in Fig. 4(a)) from the intersection point of the coordinate vector $\mathbf{r}$ with the tube inner surface, then the inner and outer surface can be represented by $z = 0$ and $z = d$, respectively. Suppose the inner radius at the certain stable growth is $r_0$, then $z = r - r_0$ (in the 1D frame $\mathbf{r}$ is scalarized), as shown in Fig. 4(a). The derivatives in Eqs. (3)–(5) remain unchanged with $z$ due to its linear relationship with $\mathbf{r}$. At the inner surface where $z = 0$, the generation of $TiO_2$ is normally zero, therefore:

$$\left(\frac{\partial[TiO_2]}{\partial t}\right)_{z=0} = -\frac{1}{6}k_1R_1([TiO_2],[F^-]) \tag{6}$$

At the outer surface of $TiO_2$ where $z = d$, the dissolution normally takes place above the bottom area, and in is weak near the bottom area. Hence in the outer surface, the change of $TiO_2$ amount can be approximately described by:

$$\left(\frac{\partial[TiO_2]}{\partial t}\right)_{z=d} = \frac{1}{2}k_2R_2([Ti^{4+}],[O^{2-}]) \tag{7}$$

When the tube growth is stable, both $(\partial[TiO_2]/\partial t)_{z=0}$ and $(\partial[TiO_2]/\partial t)_{z=d}$ will be constant. The changes of the $TiO_2$ layer by alternated conditions will be then represented by the changes of these two terms. Under room temperature, there are two situations in different voltage regimes. When the applied potential difference $\Delta V$ is lower than the upper limit (mentioned in Section 3.1), giving a small increase to $\Delta V$, the values of $k_2$, $[F^-]$ and $[O^{2-}]$ will increase according to their forms. As a result, the term $(\partial[TiO_2]/\partial t)_{z=d}$ increases by the increase of $k_2$ and $[O^{2-}]$ according to Eq. (7), while the absolute value of term $(\partial[TiO_2]/\partial t)_{z=0}$ also increases but more weakly only by the increase of $[F^-]$ according to Eq. (6), as shown in Fig. 4(a). Therefore the dissolution of the $TiO_2$ at the inner surface and generation of $TiO_2$ are both enhanced by the increasing applied potential difference. And due to the weaker increase of the absolute value of $(\partial[TiO_2]/\partial t)_{z=0}$, the net growth of the $TiO_2$ thickness $\Delta d$ is also positive. As a result, the tube size (outer diameter and wall thickness) and the growth rate increase monotonously at low applied potential difference, as indicated by the two dashed curves in Fig. 4(a). This is consistent with the relationship $D = 2f_{growth}\Delta V$ mentioned in Section 3.1. Secondly, when $\Delta V$ is increased to too high value where no tubes can be formed, as shown in Fig. 1(a)–(c), the side etching begin to appear due to the enrichment of highly mobile $F^-$ ions (compared to low temperatures) at the side of tubes. Before reaching the bottom, the $F^-$ ions are accelerated by distorted electric field in the radial direction, as shown in Fig. 4(b). As a result, destruction of tube array is induced and irregular porous structure is formed.

Under lower temperature, there are also two situations according to the applied potential difference. In the low voltage regime, the morphological behavior is also monotonous versus increasing applied potential, as shown in Fig. 4(c). But compared to the situation under room temperature at the same potential difference, $k_1$ and $k_2$ are both reduced, and the potential drop on the sample layer is lower than that under room temperature due to higher resistance of the electrolyte from lower ionization rate. Therefore the modulus of both $(\partial[TiO_2]/\partial t)_{z=d}$ and $(\partial[TiO_2]/\partial t)_{z=0}$ are reduced at two interfaces, so the tube sizes are smaller with lower temperature at fixed low $\Delta V$. However, since the etching at the end of the tubes is also reduced, the growth rate will not be significantly sacrificed and can be compensated by slightly increasing applied potential difference.

When the applied potential difference $\Delta V$ is increased to high enough value, significant enrichment of $F^-$ anions begins to take place near the outer surface of the tube bottom by field drift at high potential difference according to Eq. (3), as shown in Fig. 4(d). In the mean time, the motion of $F^-$ ions in the radial direction are limited by the electrolyte at lowed temperature according to Eq. (3), which inhibits the side etching effect that could lead to destruction of tube formation at room temperature. Due to the $F^-$ enrichment outside of the tube bottom, the dissolution also takes place near the bottom in the area between the tubes, thus the term $(\partial[TiO_2]/\partial t)_{z=d}$ is no longer in the form of Eq. (7), but Eq. (5). Hence $(\partial[TiO_2]/\partial t)_{z=d}$ is strongly reduced and tube walls shrink backward with higher $\Delta V$. As a result, the tube outer diameter decreases with increasing $\Delta V$, as indicated by the outer dashed curve in Fig. 4(d). In the mean time, due to the redistribution of $F^-$ anions to the outside, the $[F^-]$ near the inner surface of $TiO_2$ will be reduced. Therefore the absolute value of $(\partial[TiO_2]/\partial t)_{z=0}$ can decrease according to Eq. (6), and the inner diameter will decrease with increasing applied potential difference, as shown by the inner dashed curve in Fig. 4(d). The wall thickness will decrease with increasing $\Delta V$ due to the general enrichment of $F^-$ anions at the bottom position of the tube array. Furthermore, the increased $\Delta V$ also enhances the process (3) at the end of the tube through stronger drift, thus the net tube growth is reduced due to stronger dissolution at the top and weaker oxidation at the bottom. The inhibition of the side etching effect induces the increase of the upper limit of $\Delta V$ to form tubular $TiO_2$ structures, as shown in Fig. 1(a)–(c). As the inhibition of side etching will be stronger at lower temperature, the tubes can be formed at higher applied potential difference.

According to the above discussion, the optimized condition to form small tubes could be realized by simply tuning the applied potential difference $\Delta V$ and the temperature $T$. Firstly, as $\Delta V$ is lowered, influence from the electric field in the radial direction becomes relatively weaker than from the temperature which decides the diffusion and mobility of the ions. If only $\Delta V$ is reduced, as the vertical motion of ions toward the bottom weakened by reduced vertical drift, the radical motion is still significant by diffusion (second terms in Eqs. (3) and (4)), thus the size reduction in radial direction is limited. If $\Delta V$ is further decreased, the tube bottom becomes more and more flat, until finally grow simply compact oxide layer. But secondly, if the temperature also declines while decreasing $\Delta V$, the oxide growth in radial direction will be further reduced, then smaller tubes can be achieved. Nevertheless, when the temperature is too low, the oxide dissolution is inhibited, thus the tubes also cannot be formed. Therefore, the optimal condition of the temperature and the applied potential difference to form



Please cite this article in press as: H. Liu, et al., Optimal self-organized growth of small anodic $TiO_2$ nanotubes with "micro-annealing" effect under complex conditions via reaction–diffusion approach, Electrochim. Acta (2011), doi:10.1016/j.electacta.2011.02.029

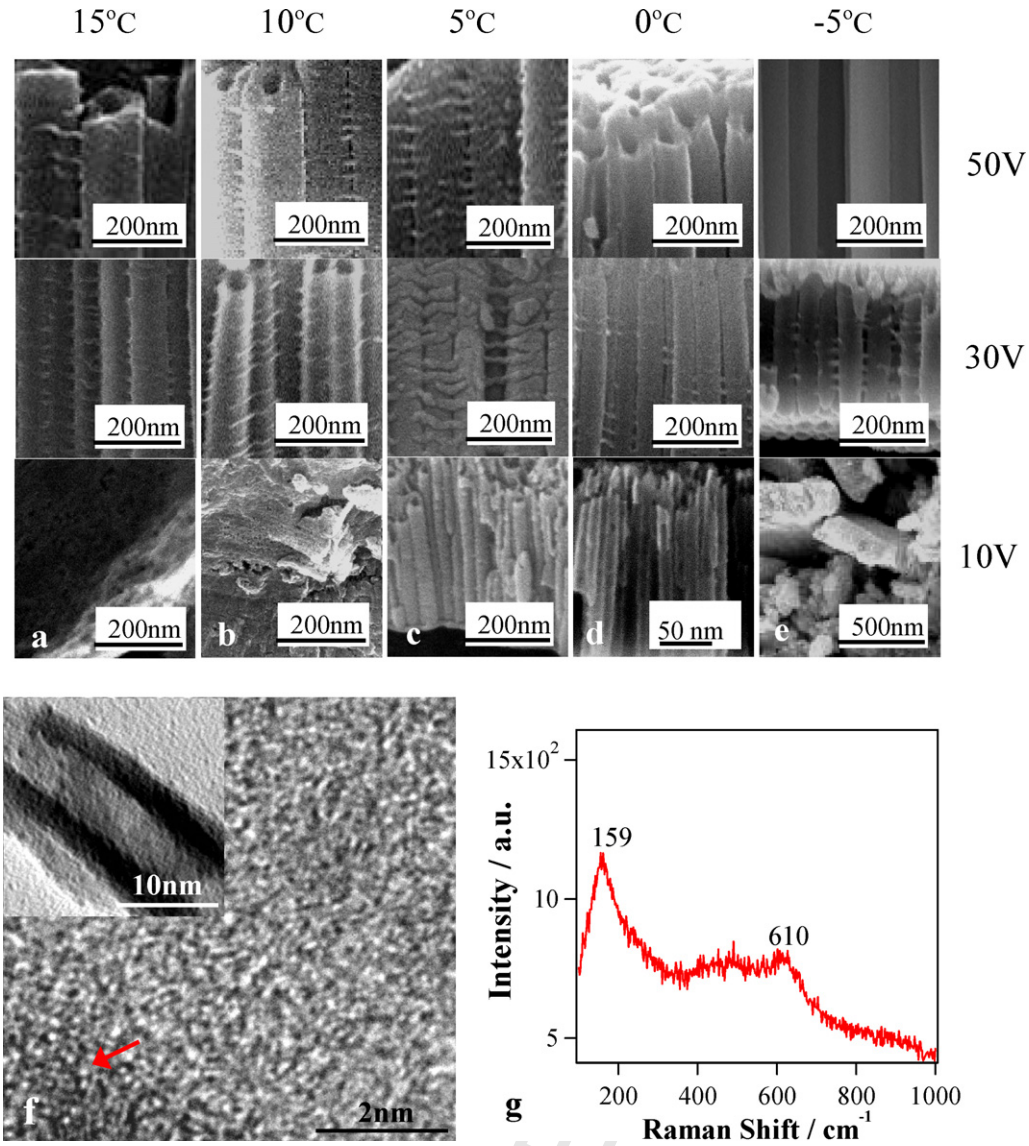


**Fig. 5.** Approaching ultrasmall $TiO_2$ tubes with varied temperature and applied potential difference, in ethylene glycol with 1.0 vol.% $H_2O$, 0.09 M $NH_4F$, shown by SEM cross-sectional images, under temperatures: (a) 15 °C, (b) 10 °C, (c) 5 °C, (d) 0 °C, and (e) −5 °C. (f) TEM image of the ultrasmall $TiO_2$ tube at 0 °C and 10 V, red arrow indicates the area where atoms tend to be organized. (g) Raman spectrum of the as-prepared smallest $TiO_2$ tube at 0 °C, 10 V. (For interpretation of the references to color in this figure legend, the reader is referred to the web version of this article.)

ultrasmall tubes will be certain medium values in the middle left region in the phase diagrams in Fig. 1(a)–(c).

### 3.4. Optimal growth of ultrasmall $TiO_2$ tube arrays

As exhibited in previous sections, the $TiO_2$ tube growth has shown some unconventional size evolution in a wide condition range, and in the mechanism discussion where the reaction–diffusion method has been applied, the optimal condition to form ultrasmall (~10 nm) tube arrays has been discussed. It has also been found that temperature controlling could induce significant "micro-annealing" effect in the as-prepared $TiO_2$ tubes. Now we show in Fig. 5(a)–(e) more detailed experimental approach to realize the optimized growth of ultrasmall tube arrays with good quality and fast growth rate.

On one hand, under constant temperature, the tube size decreases with decreasing applied potential difference $\Delta V$ until the lower limit is reached and only oxide layer is formed. For example, in E.G. (with 1.0 vol.% $H_2O$ and 0.09 M $NH_4F$), the smallest tubes at 15 °C were obtained at 30 V with the size of outer diameter $D$ = 90 nm, which indicated the reduction of the tube size is limited if only the applied potential difference is reduced. On the other hand, at constant $\Delta V$, the tube diameter generally decreased with the decreasing temperature from 15 to 0 °C. When the temperature decreased from 0 to −5 °C, the tube size continued to decrease when $\Delta V \geq 10$ V, but when $\Delta V < 10$ V, no significant tube arrays were detected except oxide films. Thus it can be concluded that the optimal temperature regime is ~0 °C to grow uniform ultrasmall ($D$ ~ 10 nm) $TiO_2$ tubes under low applied potential difference, as shown in Fig. 5(d). Compared to the previously fabricated tubes with similar sizes [21,31], these ultrasmall tubes are better ordered, with thin wall thickness (~3 nm) and high growth rate (~0.3–0.4 μm $h^{-1}$).

Afterwards, detailed structural studies on these as-prepared ultrasmall $TiO_2$ tubes have been carried out by TEM and Raman scattering spectroscopy. The nanometer-sized grains with well ordered structure previously studied in larger tubes (shown in Fig. 3(b)) were hard to be detected in these ultrasmall tubes, as shown by the high resolution TEM image in Fig. 5(f). However, atoms have begun to be organized in some area (indicated by red

arrow) as shown in Fig. 5(f), and the Raman spectrum in Fig. 5(g) has indicated existence of small grains in a larger scale, with peaks at 159 and 610 $cm^{-1}$ which are related to the nanocrystal $TiO_2$ with anatase and rutile phases, respectively [10,45]. Above results have shown that although the nanometer-sized grains are not easily found due to possible size limit by the very thin tube wall (~3 nm), the as-prepared ultrasmall nanotubes are quite ordered in general and have some organized microstructures already. Generally combined adjustment of the temperature and the applied potential is suitable to control the $TiO_2$ tube sizes, and to reach optimal conditions (~0 °C, ~10 V) for ultrasmall tubes with more ordered microstructure by reducing the applied potential difference without changing other factors like the electrolyte concentration.

## 4. Conclusions

To summarize this paper, we have systematically investigated the complex behavior (size, growth rate, and ordering) of the $TiO_2$ tube formation in the anodic oxidation system in highly viscous electrolyte (E.G., with 1.0 vol.% $H_2O$ and 0.09 M $NH_4F$) with varied applied potential difference and temperature. The morphological properties of the system, such as the nonmonotonous change of size and growth rate versus the applied potential difference and the temperature have been carefully investigated in a very wide experimental range. Such behaviors have been in general qualitatively discussed with a reaction–diffusion model including the reaction, diffusion, and field drift processes of three main species ($F^-$, $O^{2-}$ and $TiO_2$). Moreover, evidences have shown that the formation of small (~2–10 nm) crystal grains with anatase or rutile structure can be enhanced in the as-prepared $TiO_2$ tube wall under decreasing temperatures. Due to its relationship to the temperature and similarity to the annealing at higher temperatures of several hundred centigrade, we name this phenomenon "micro-annealing", which might be useful in general electrochemical fabrication method of the $TiO_2$ material [7–10].

Finally, the optimized growth under complex conditions for small tubes with specific size has been realized, for example, the ultrasmall (outer diameter $D \sim 10$ nm, wall thickness $d \sim 3$ nm) and small ($D \sim 50$–$90$ nm, $d \sim 15$ nm) $TiO_2$ tubes have been fabricated with high growth rate and structural quality. Introduction of the reaction–diffusion method to the nanotube formation process appeared to be helpful to understand more details in the nanostructure formation of $TiO_2$. The experimental results will be helpful to develop devices based on $TiO_2$ tubes with controllable sizes and nanocrystal structures for certain properties, for example, the tubes formed at low temperatures have shown interesting cathodoluminescence properties [49].

## Acknowledgements

This work was supported by the National Major Basic Research Project of 2010CB933702, Natural Science Foundation of China under contract 10734020, and Shanghai Municipal Commission of Science and Technology Project of 08XD14022.

## References

[1] B. O'Regan, M. Gräztel, Nature 353 (1991) 737.
[2] G.K. Mor, K. Shandar, M. Paulose, O.K. Varghese, C.A. Grimes, Nano Lett. 6 (2006) 215.
[3] A. Fujishima, K. Honda, Nature 238 (1972) 37.
[4] S.P. Albu, A. Ghicov, J.M. Macak, P. Schmuki, Nano Lett. 7 (2007) 1286.
[5] M. Kitao, Y. Oshima, K. Urabe, Jpn. J. Appl. Phys. Part 1 36 (1997) 4423.
[6] H. Tsuchiya, J.M. Macak, L. Müller, J. Kunze, F. Müller, P. Greil, S. Virtanen, P. Schmuki, J. Biomed. Mater. Res. Part A 77A (2006) 534.
[7] K. Nagaveni, M.S. Hegde, N. Ravishankar, G.N. Subbanna, G. Madras, Langmuir 20 (2004) 2900.
[8] G.L. Tian, H.B. He, J.D. Shao, Chin. Phys. Lett. 22 (2005) 1787.
[9] N.K. Shrestha, M. Yang, Y.C. Nah, I. Paramasivam, P. Schmuki, Electrochem. Commun. 12 (2010) 254.
[10] S. Balaji, Y. Djaoued, J. Robichaud, J. Raman Spectrosc. 37 (2006) 1416.
[11] A. Ghicov, P. Schmuki, Chem. Commun. (2009) 2791.
[12] P. Roy, D. Kim, K. Lee, E. Spiecker, P. Schmuki, Nanoscale 2 (2010) 45.
[13] J.M. Macak, P. Schmuki, Electrochim. Acta 52 (2006) 1258.
[14] J.M. Macak, H. Tsuchiya, L. Taveira, A. Aldabergerova, P. Schmuki, Angew. Chem. Int. Ed. 44 (2005) 7463.
[15] J. Wang, Z.Q. Lin, Chem. Mater. 20 (2008) 1257.
[16] G.A. Crawford, N. Chawla, Acta Mater. 57 (2009) 854.
[17] H.E. Prakasam, K. Shankar, M. Paulose, O.K. Varghese, C.A. Grimes, J. Phys. Chem. C 111 (2007) 7235.
[18] M. Paulose, H.E. Prakasam, O.K. Varghese, L. Peng, K.C. Popat, G.K. Mor, T.A. Desari, C.A. Grimes, J. Phys. Chem. C 111 (2007) 14992.
[19] S.P. Albu, A. Ghicov, J.M. Macak, P. Schmuki, Phys. Stat. Sol. (RRL) 1 (2007) R65.
[20] M. Paulose, K. Shankar, S. Yoriya, H.E. Prakasam, O.K. Varghese, G.K. Mor, T.A. Latempa, A. Fitzgerald, C.A. Grimes, J. Phys. Chem. B 110 (2006) 16179.
[21] J.M. Macak, M. Zlamal, J. Krysa, P. Schmuki, Small 3 (2007) 300.
[22] A. Valota, D.J. LeClere, P. Skeldon, M. Curioni, T. Hashimoto, S. Berger, J. Kunze, P. Schmuki, G.E. Thompson, Electrochim. Acta 54 (2009) 4321.
[23] X.B. Chen, M. Schriver, T. Suen, S.S. Mao, Thin Solid Films 515 (2007) 8511.
[24] S. Rani, S.C. Roy, M. Paulose, O.K. Varghese, G.K. Mor, S. Kim, S. Yoriya, T.J. LaTempa, C.A. Grimes, Phys. Chem. Chem. Phys. 12 (2010) 2780.
[25] S. Berger, J. Kunze, P. Schmuki, A.T. Valota, D.J. Leclere, P. Skeldon, G.E. Thompson, J. Electrochem. Soc. 157 (2010) C18.
[26] Y.-Y. Song, P. Schmuki, Electrochem. Commun. 12 (2010) 579.
[27] H. Yin, H. Liu, W.Z. Shen, Nanotechnology 21 (2010) 035601.
[28] K. Yasuda, J.M. Macak, S. Berger, A. Ghicov, P. Schmuki, J. Electrochem. Soc. 154 (2007) C472.
[29] J.M. Macak, H. Tsuchiya, A. Ghicov, K. Yasuda, R. Hahn, S. Bauer, P. Schmuki, Curr. Opin. Solid State Mater. Sci. 11 (2007) 3.
[30] J.M. Macak, H. Hildebrand, U. Marten-Jahns, P. Schmuki, J. Electroanal. Chem. 621 (2008) 254.
[31] S.P. Albu, D. Kim, P. Schmuki, Angew. Chem. Int. Ed. 47 (2008) 1916.
[32] L.V. Taveira, J.M. Macak, K. Sirotna, L.F.P. Dick, P. Schmuki, J. Electrochem. Soc. 153 (2006) B137.
[33] S.P. Albu, A. Ghicov, S. Aldabergenova, P. Drechsel, D. LeClere, G.E. Thompson, J.M. Macak, P. Schmuki, Adv. Mater. 20 (2008) 4135.
[34] S. Yoriya, G.K. Mor, S. Sharma, C.A. Grimes, J. Mater. Chem. 18 (2008) 3332.
[35] J. Wang, Z.Q. Lin, J. Phys. Chem. C 113 (2009) 4026.
[36] W.G. Bessler, Solid State Ionics 176 (2005) 997.
[37] R. Imbihl, G. Ertl, Chem. Rev. 95 (1995) 697.
[38] R. Imbihl, Handbook of Surface Science, vol. 3, Elsevier, Oxford, UK, 2008 (Chapter 9).
[39] A. Bieberle, L.J. Gauckler, Solid State Ionics 146 (2002) 23.
[40] Y.B. Nian, J. Strozier, N.J. Wu, X. Chen, A. Ignatiev, Phys. Rev. Lett. 98 (2007) 146403.
[41] S. Kotsantonis, J.A. Kilner, Solid State Ionics, in press. Q1
[42] A.H. Heuer, K.P.D. Lagerlof, Philos. Mag. Lett. 79 (1999) 619.
[43] S. Berger, H. Tsuchiya, P. Schmuki, Chem. Mater. 20 (2008) 3245.
[44] D.T. Cromer, K. Herrington, J. Am. Chem. Soc. 77 (1955) 4708.
[45] P.J. Huang, H. Chang, C.T. Yeh, C.W. Tsai, Thermochim. Acta 297 (1997) 85.
[46] S.K. Poznyak, D.V. Talapin, A.I. Kulak, J. Electr. Chem. 579 (2005) 299.
[47] Fluid Properties Calculator. www.mhtl.uwaterloo.ca/old/onlinetools/airprop/air prop.html (accessed 26.10.10).
[48] T. Shimizu, E. Kenndler, Electrophoresis 20 (1999) 3364.
[49] M. Enachi, M. Stevens-Kalceff, I. Tiginyanu, V. Ursaki, Mater. Lett. 64 (2010) 2155.